MOLECULAR PHYSICS, 1994, VOL. 81, NO. 3, 579–598

Non-additive intermolecular forces from the spectroscopy of van der Waals trimers: far-infrared spectra and calculations on Ar_2–DCl

By MATTHEW J. ELROD and RICHARD J. SAYKALLY
Department of Chemistry, University of California, Berkeley, California 94720, USA

ADAM R. COOPER and JEREMY M. HUTSON
Department of Chemistry, University of Durham, South Road, Durham DH1 3LE, England

(*Received 8 July 1993; accepted 9 August 1993*)

The far-infrared vibration–rotation spectrum of the out-of-plane DCl bending band of Ar_2–DCl is observed around 36·0 cm^{-1}. The experimental bending frequency, rotational constants and hyperfine coupling constants are compared with the results of calculations employing both pairwise-additive and non-additive interaction potentials. As found previously for Ar_2–HCl, there are substantial discrepancies between the experimental results and calculations employing a pairwise-additive potential. To explain the discrepancy it is necessary to include a non-additive term that arises from the interaction of the permanent multipoles of the DCl monomer with an overlap-induced quadrupole on Ar_2. The new spectra should prove very valuable in a future determination of the non-additive contribution to the potential.

1. Introduction

There has been much recent experimental and theoretical interest in the spectroscopy of van der Waals trimers such as Ar_2–HCl. Such trimers form a bridge between studies of interaction potentials in gases and in condensed phases. The intermolecular pair potentials for Ar–Ar and Ar–HCl are known very accurately [1–4], so that studies of the trimer spectra can for the first time provide rigorous and detailed information on non-additive (three-body) forces in molecular systems.

The Ar_2–HCl trimer was first observed experimentally by Klots *et al.* [5], using Fourier transform microwave spectroscopy in a supersonic jet. They established that the ground-state geometry was triangular, with the HCl molecule executing wide-amplitude vibrations about a C_{2v} geometry in which the HCl molecule was orientated towards the midpoint of the two Ar atoms. Subsequently, Hutson *et al.* [6] carried out approximate calculations of the bound states of Ar_2–HCl in three dimensions, neglecting Ar–Ar vibrational degrees of freedom, and showed that the spectra were sensitive to non-additive contributions to the intermolecular potential. However, they concluded that the microwave spectra alone did not contain sufficient information to determine the non-additive forces, and made predictions of the locations of excited states correlating with hindered internal rotation of HCl in the complex. Three different HCl bending bands were predicted in the far-infrared.

The early theoretical work stimulated experimental interest in the far-infrared spectrum of Ar_2–HCl. Elrod *et al.* [7–9] succeeded in measuring the spectra of all three of the HCl bending bands, using tunable far-infrared laser spectroscopy. In

parallel with this, Cooper and Hutson [10] developed a method for solving the full five-dimensional equations to calculate the vibrational levels, and compared the experimental vibrational frequencies with the results of calculations using a variety of pairwise-additive and non-additive potential energy surfaces. They found substantial discrepancies (up to $2\,cm^{-1}$) between the experimental frequencies and those calculated from pairwise-additive potentials. The usual non-additive terms used for triatomic systems (such as the Axilrod–Teller triple-dipole term) were not capable of reproducing these frequency shifts, even when their anistropy was included. However, Cooper and Hutson identified a new non-additive term which qualitatively explains the discrepancies. The term arises from the interaction between the permanent multipoles of the HCl molecule and the overlap-induced quadrupole that develops on an Ar_2 pair at short range. It is related to the exchange quadrupole-induced dipole (EQID) mechanism that is believed to be responsible for the absorption of far-infrared radiation by rare gas liquids [11]. Non-additive forces of this type may be expected to be a general feature of molecular (as opposed to atomic) interactions.

We hope in the future to be able to *extract* detailed information on the non-additive forces from the vibration–rotation spectra. However, more experimental results are needed before this will be possible. For van der Waals dimers such as Ar–HCl and Ar–HF, it has been found that the spectra of deuterated species contain important additional information on the potential energy surface. This is because DCl and DF have substantially smaller rotational constants than HCl and HF, so that the corresponding complexes have bending wavefunctions that sample significantly different parts of the potential energy surface. The microwave spectrum of Ar_2–DCl has been observed by Klots and Gutowsky [12], and it is of great interest to investigate the far-infrared spectrum.

The coordinate system used for Ar_2–HCl or Ar_2–DCl is shown in figure 1. The positions of the two Ar atoms and the DCl centre of mass are described by a set of Jacobi coordinates: the Ar–Ar distance is denoted ρ, the distance from the DCl centre of mass to the Ar_2 centre of mass is denoted R, and the angle between the vectors corresponding to R and ρ is denoted χ. The DCl bond length is denoted r, and the angle between the r and R vectors is θ, with $\theta = 0$ corresponding to the D atom of DCl pointing directly towards the Ar_2 centre of mass. Finally, the angle ϕ is the torsional angle between the r and ρ axes, viewed along R: $\theta = 0$ corresponds to DCl lying in the plane of the heavy atoms, while $\phi = 90°$ is the out-of-plane geometry.

In a complex such as Ar–DCl or Ar_2–DCl, the DCl molecule executes hindered

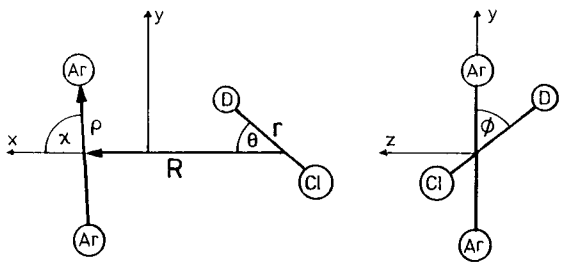

Figure 1. Coordinate system used for Ar_2–HCl.

rotational motion under the influence of the anisotropic intermolecular potential. The motion is more hindered for DCl complexes than for HCl complexes, because of the smaller rotational constant of DCl. Nevertheless, the DCl internal rotor quantum number j is still a useful label. In Ar–HCl or Ar–DCl, the lowest excited states correlate with $j = 1$, and have a well-defined projection quantum number K onto the intermolecular axis. The $j = 1\,\Pi$ states, with $|K| = 1$, form a degenerate pair split only by l-type doubling arising from Coriolis coupling with $K = 0$ states. The $j = 0$, $K = 0$ and $j = 1$, $K = 0$ free-rotor states are strongly mixed by the potential anistropy: the ground state may be thought of qualitatively as the positive linear combination of the two, and is concentrated around $\theta = 0$; the Σ bend excited state is qualitatively the negative linear combination, and is concentrated around $\theta = 180°$.

The DCl bending states in Ar_2–DCl are similar in character, except that (i) the projection of j onto R is denoted k, and is no longer the only contribution to K_a (the projection of J onto R), and (ii) the even and odd linear combinations of $k = +1$ and $k = -1$, corresponding to in-plane (B_2) and out-of-plane (B_1) motions of the DCl, are split by potential coupling instead of just Coriolis coupling. There is still a Σ bending state, correlating with DCl $j = 1$, $k = 0$, which is concentrated around $\theta = 180°$.

2. Experimental method

The far-infrared vibration–rotation–tunneling spectrum of Ar_2–DCl was observed in a continuous supersonic planar jet expansion probed by a tunable far-infrared laser spectrometer. The spectrometer has been described in detail previously [13], so only a brief description will be given here. The tunable far-infrared radiation is generated by mixing an optically pumped line-tunable far-infrared gas laser with continuously tunable frequency-modulated microwaves in a Schottky barrier diode to generate light at the sum and difference frequencies ($\nu = \nu_{FIR} \pm \nu_{MW}$). The tunable radiation is separated from the much stronger fixed-frequency radiation with a Michelson polarizing interferometer, and is then directed to multi-pass optics which encompass the supersonic expansion. After passing 10 times through the expansion, the radiation is detected by a liquid-helium-cooled Putley-mode InSb detector, and the signal is demodulated at $2f$ by a lock-in amplifier.

$Ar_n(DCl)_m$ clusters were produced by continuously expanding a mixture of 0·5% DCl in argon at a stagnation pressure of 2 atm through a 10 cm × 25μm slit nozzle planar jet into a vacuum chamber pumped by a 1200 ls^{-1} Roots pump. For this study, DCl was synthesized by reaction of D_2O with benzoyl chloride [14], cryogenically distilled with liquid nitrogen, and used with no further purification. The following far-infrared laser lines provided the fixed-frequency radiation: 1016·8972 GHz CH_3OD, 1042·1504 GHz CH_2F_2, 1101·1594 GHz CH_2DOH and 1110·3199 GHz CH_2F_2.

3. Experimental results and analysis

The out-of-plane bend of Ar_2–DCl was observed around 36 cm^{-1}. It is characterized by strong c-type Q-branch transitions. Because of spectral congestion, rotational/nuclear hyperfine combination differences [9] calculated from the Fourier transform microwave spectra of Klots and Gutowsky [12] were used to assign rotational quantum numbers to the far-infrared spectra. Although the experimental

Table 1. Observed transitions and residuals for Ar_2–$D^{35}Cl$.

$J_{KpKo'} \leftarrow J_{KpKo''}$	Frequency/MHz	(Observed–calculated)/MHz
$1_{11} \leftarrow 1_{01}$	1080777·5	−1·1
$2_{12} \leftarrow 3_{22}$	1070574·7	1·3
$2_{12} \leftarrow 2_{02}$	1080737·8	−0·5
$3_{13} \leftarrow 3_{03}$	1080801·3	−1·2
$3_{31} \leftarrow 4_{41}$	1067404·9	1·3
$3_{31} \leftarrow 2_{21}$	1091408·3	−1·0
$4_{14} \leftarrow 5_{24}$	1063979·1	1·7
$4_{14} \leftarrow 4_{04}$	1080892·1	−0·3
$5_{15} \leftarrow 5_{05}$	1080999·5	−0·2
$5_{50} \leftarrow 6_{60}$	1061314·8	−2·8
$5_{50} \leftarrow 4_{40}$	1098837·2	1·5
$6_{15} \leftarrow 7_{25}$	1057699·2	2·6
$6_{15} \leftarrow 6_{25}$	1081363·9	−0·2
$6_{16} \leftarrow 6_{06}$	1081124·0	0·1
$6_{52} \leftarrow 7_{62}$	1058228·9	2·6
$7_{16} \leftarrow 8_{26}$	1054504·7	1·4
$7_{16} \leftarrow 7_{26}$	1081549·9	0·4
$7_{16} \leftarrow 6_{06}$	1105228·0	0·2
$7_{17} \leftarrow 8_{27}$	1054208·5	1·9
$7_{17} \leftarrow 7_{07}$	1081264·8	−0·2
$7_{34} \leftarrow 7_{44}$	1081946·6	−4·3
$7_{35} \leftarrow 8_{45}$	1054747·4	−2·6
$7_{35} \leftarrow 7_{25}$	1081778·5	−4·0
$7_{35} \leftarrow 6_{25}$	1105446·7	−3·4
$7_{53} \leftarrow 6_{43}$	1105773·8	−0·9
$7_{70} \leftarrow 8_{80}$	1055585·3	1·9
$7_{70} \leftarrow 6_{60}$	1106924·2	0·7
$7_{71} \leftarrow 8_{81}$	1055605·2	−0·6
$7_{71} \leftarrow 6_{61}$	1107095·7	−2·1
$8_{17} \leftarrow 9_{27}$	1051332·1	3·9
$8_{17} \leftarrow 8_{27}$	1081752·0	0·5
$8_{17} \leftarrow 7_{07}$	1108811·0	1·0
$8_{18} \leftarrow 8_{08}$	1081423·1	0·2
$8_{36} \leftarrow 9_{46}$	1051622·1	1·9
$8_{36} \leftarrow 8_{26}$	1082028·1	−0·4
$8_{71} \leftarrow 9_{81}$	1052377·8	0·7
$8_{71} \leftarrow 7_{61}$	1109522·2	−2·3
$9_{18} \leftarrow 9_{28}$	1081970·9	0·8
$9_{18} \leftarrow 8_{08}$	1112409·5	1·7
$9_{19} \leftarrow 9_{09}$	1081597·0	−0·6
$9_{36} \leftarrow 10_{46}$	1048790·4	−3·5
$9_{37} \leftarrow 9_{27}$	1082291·0	0·2
$9_{37} \leftarrow 8_{27}$	1112715·2	1·1
$10_{19} \leftarrow 11_{29}$	1045033·4	1·1
$10_{19} \leftarrow 10_{29}$	1082205·4	0·2
$10_{110} \leftarrow 10_{010}$	1081778·5	−0·8
$10_{37} \leftarrow 11_{47}$	1045746·8	0·8
$10_{37} \leftarrow 10_{47}$	1082877·3	−2·7
$10_{37} \leftarrow 9_{27}$	1116660·3	−1·7
$10_{38} \leftarrow 10_{28}$	1082570·6	1·4
$11_{110} \leftarrow 12_{210}$	1041912·7	1·3
$11_{110} \leftarrow 11_{210}$	1082457·2	0·4
$11_{111} \leftarrow 11_{011}$	1081996·3	−0·5

Table 1. Continued

$J_{KpKo'} \leftarrow J_{KpKo''}$	Frequency/MHz	(Observed–calculated)/MHz
$11_{38} \leftarrow 12_{48}$	1042717·2	1·0
$11_{38} \leftarrow 11_{48}$	1083217·7	0·3
$11_{38} \leftarrow 10_{28}$	1120372·6	1·5
$11_{39} \leftarrow 12_{49}$	1042343·7	3·1
$11_{39} \leftarrow 10_{29}$	1120039·9	3·2
$12_{111} \leftarrow 12_{211}$	1082724·4	−0·4
$12_{112} \leftarrow 12_{012}$	1082219·6	−1·5
$12_{39} \leftarrow 13_{49}$	1039707·5	3·0
$12_{39} \leftarrow 12_{49}$	1083571·9	1·5
$13_{112} \leftarrow 13_{212}$	1083008·5	−0·6
$13_{113} \leftarrow 13_{013}$	1082460·4	−1·5
$13_{310} \leftarrow 13_{410}$	1083942·0	3·1
$13_{59} \leftarrow 13_{49}$	1084318·4	−3·6
$14_{113} \leftarrow 14_{213}$	1083308·8	−0·7
$14_{114} \leftarrow 14_{014}$	1082717·3	−1·7
$14_{311} \leftarrow 14_{411}$	1084324·2	1·4
$14_{510} \leftarrow 14_{410}$	1084745·8	−1·2
$15_{115} \leftarrow 15_{015}$	1082990·8	−1·4
$15_{511} \leftarrow 15_{411}$	1085187·6	1·0
$16_{115} \leftarrow 16_{215}$	1083956·1	−2·4
$16_{116} \leftarrow 16_{016}$	1083281·7	0·2
$17_{117} \leftarrow 17_{017}$	1083586·5	−0·2
$18_{117} \leftarrow 18_{217}$	1084667·1	−3·5
$18_{118} \leftarrow 18_{018}$	1083908·4	0·6
$19_{119} \leftarrow 19_{019}$	1084245·0	0·6
$20_{120} \leftarrow 20_{020}$	1084598·9	2·4
Pure rotational transitions (included in fit)		
$1_{01} \leftarrow 0_{00}$	2492·142	−0·001
$2_{02} \leftarrow 1_{01}$	4250·328	−0·001
$2_{20} \leftarrow 1_{01}$	7673·393	0·000
$3_{22} \leftarrow 3_{03}$	4267·189	0·000
$3_{03} \leftarrow 2_{02}$	5897·662	0·000
$3_{22} \leftarrow 2_{21}$	7475·494	0·001
$3_{21} \leftarrow 2_{20}$	9053·255	0·000
$4_{04} \leftarrow 3_{03}$	7575·344	0·000
$4_{23} \leftarrow 3_{22}$	9265·624	0·000
$4_{22} \leftarrow 3_{21}$	11146·211	0·000
$5_{05} \leftarrow 4_{04}$	9255·600	0·000
$5_{24} \leftarrow 4_{23}$	10957·490	0·000

sensitivity was sufficient to observe transitions from the Ar_2–$D^{37}Cl$ isotopic species, the lack of microwave data prevented the use of this rigorous assignment technique and, consequently, no far-infrared spectra were assigned for this isotopomer.

The hyperfine-free line centres (see table 1) and the pure rotational transitions were simultaneously fitted to a Watson S-reduced Hamiltonian [15]. Although the experimental resolution of approximately 500 kHz was sufficient to observe the chlorine nuclear quadrupole hyperfine structure, the effects due to deuterium quadrupole coupling were not resolvable and were therefore neglected in the hyperfine analysis. Because of the values of the upper state nuclear hyperfine coupling constants, it was possible to resolve all four of the strong $\Delta F = \Delta J$ hyperfine

Table 2. Molecular constants and angular expectation values (1σ uncertainties).

Ar_2–$D^{35}Cl$	Ground state	Out-of-plane-bend
ν_o/cm^{-1}		36·04605(2)
B_x/MHz	1735·0953(12)	1788·14(18)
B_y/MHz	1651·6647(18)	1662·76(15)
B_z/MHz	840·5010(4)	849·021(10)
D_J/kHz	23·50(6)	31·7(4)
D_{JK}/kHz	−39·85(16)	−54·6(7)
D_K/kHz	18·20(10)	25·0(4)
d_1/kHz	2·55(6)	10·6(14)
d_2/kHz	−0·351(16)	−14·9(4)
Rotational RMS error/MHz	1·7	
χ_{xx}/MHz	−38·1840(7)	−12·77(14)
χ_{yy}/MHz	17·4533(8)	17·83(14)
χ_{zz}/MHz	20·7307(8)	−5·06(10)
$\langle P_2(\cos\theta)\rangle$	0·566583(10)	0·189(2)
$\langle\Delta(\theta,\phi)\rangle$	0·032420(16)	−0·226(2)

components for a large number of rovibrational transitions. The nuclear hyperfine structure was separately fitted using a Hamiltonian calculated in the coupled basis set $|JKIF\rangle$ [16], where $F = I + J$ and $I = \frac{3}{2}$ for ^{35}Cl. The molecular constants resulting from both the rotational and nuclear hyperfine fits are reported in table 2.

The vibrational assignment was determined from the observed selection rules and the values of the nuclear quadrupole coupling constants. The vibrationally averaged ground state of Ar_2–DCl is a planar T-shaped asymmetric top of C_{2v} symmetry. The observed c-type selection rules dictate that transitions from an A_1 ground state must terminate in a B_1 upper state. The out-of-plane bend is expected to be the only low-lying (below 50 cm^{-1}) vibration of B_1 symmetry. In addition, the measured nuclear quadrupole coupling constants reveal the vibrationally averaged angular orientation of the DCl constituent. The coupling constants are related to angular expectation values for the DCl motion by

$$\chi_{xx} = \chi_{DCl}\langle P_2(\cos\theta)\rangle; \tag{1}$$

$$\chi_{yy} = \chi_{zz} = \tfrac{3}{2}\chi_{DCl}\langle\Delta(\theta,\phi)\rangle, \tag{2}$$

where $P_2(\cos\theta)$ is the second Legendre polynomial and $\Delta(\theta,\phi) = \sin^2\theta\cos 2\phi$. The deviation of $\langle P_2(\cos\theta)\rangle$ from unity is a measure of the bending amplitude of the DCl monomer, whereas the deviation of $\langle\Delta(\theta,\phi)\rangle$ from zero characterizes the anisotropy of the DCl torsional motion (positive values indicating in-plane localization and negative values indicating out-of-plane localization). The observed expectation value $\langle\Delta(\theta,\phi)\rangle = -0{\cdot}226$ confirms that the assignment of the vibration to the out-of-plane bend is correct.

Similar vibration–rotation spectra of Ar_2–HCl have indicated the possibility of significant dynamic contributions (Coriolis coupling) to the experimental rotational constants, thus rendering a structural interpretation invalid [9]. If the Coriolis coupling is strong, the perturbation is manifested in the fitting process by large rotational residuals resulting from the neglect of explicit vibration–rotation interaction terms in the effective rotational Hamiltonian. However, in the case of weak coupling, the

parameters of the rotational Hamiltonian are often flexible enough to allow an accurate representation of the observed energy levels, although the molecular constants are no longer structurally meaningful. The experimental B_x rotational constant determined in this work for the out-of-plane bend of Ar_2–DCl is significantly larger than expected on purely structural grounds. In the limit of weak potential mixing between the DCl bending motions and the heavy-atom vibrations, the B_x rotational constant should be not changed greatly from the ground state upon excitation to the out-of-plane bend. Although the RMS error of the rotational fit is within the estimated experimental uncertainty (1·7 MHz), it may be noted that the off-diagonal distortion constants d_1 and d_2 are much larger for the out-of-plane bend than for the ground state. It is therefore likely that the fitted molecular constants are affected significantly by Coriolis coupling, so that comparisons with 'structural' rotational constants from vibrational calculations must be made with caution.

4. Computational method

The computational method used here is similar to that used in [10], and will be described only briefly here. The principal change in the present paper is that a slightly different basis set of Ar_2 bending and stretching functions is used, in order to give a better representation of the doubly excited heavy-atom vibrational states.

The coordinate system used is a diatom–diatom system, as described above and shown in figure 1. In the present work, the r coordinate is separated out adiabatically, and is not treated explicitly. This is a good approximation, because the DCl stretching frequency is a factor of about 50 higher than the intermolecular bending and stretching frequencies of interest here. The Ar–HCl pair potential was also determined within this approximation [4], and is known as a function of the HCl/DCl mass-reduced quantum number $\eta = (v + \frac{1}{2})/\mu_{HCl}^{1/2}$.

The vibrational Hamiltonian of Ar_2–HX in this coordinate system is [10]

$$\begin{aligned}\hat{H}_{vib} = &-\frac{\hbar^2}{2\mu R}\left(\frac{\partial^2}{\partial R^2}\right)R - \frac{\hbar^2}{M_{Ar}\rho}\left(\frac{\partial^2}{\partial \rho^2}\right)\rho \\ &+ \left(\frac{\hbar^2}{M_{Ar}\rho^2} + \frac{\hbar^2}{2\mu R^2}\right)\frac{\partial}{\partial \cos\chi}\left[(1-\cos^2\chi)\frac{\partial}{\partial \cos\chi}\right] \\ &+ \left(b_{HX} + \frac{\hbar^2}{2\mu R^2}\right)\hat{j}_{HX}^2 + V(R,\rho,\chi,\theta,\phi),\end{aligned} \tag{3}$$

where μ is the reduced mass of the diatom–diatom complex, $\mu = 2M_{Ar}M_{HX}/(2M_{Ar} + M_{HX})$, $\hat{j}_{HX}$ is the body-fixed angular momentum operator for the rotation of HX in the complex, b_{HX} is the HX rotational constant, and $V(R,\rho,\chi,\theta,\phi)$ is the complete intermolecular potential. The vibrational problem is solved by diagonalizing a single Hamiltonian matrix using a non-orthogonal basis set as described in [10]. The basis functions used are as follows. (i) A distributed Gaussian basis set [17] (DGB) is used for the R coordinate. N_i Gaussian functions $\psi_i(R)$ are distributed on an equally-spaced grid between limits R_{min} and R_{max}. (ii) Orthonormal sets of suitably adapted 1-dimensional functions are used for the ρ and χ coordinates. The basis functions $\Upsilon_w(\rho)$ and $\Phi_u(\cos\chi)$ are defined as eigenfunctions of effective potentials for the ρ and χ motions, as described below. The

resulting product basis set is restricted by the conditions $w \leq w_{\max}$ and $w + u \leq q_{\max}$. (iii) Body-fixed spherical harmonics $Y_{jk}(\theta, \phi)$ are used to describe the angular motion of the HX molecule.

The vibrational basis functions may be classified according to their symmetry (+1 or −1) under exchange of the two argon atoms, (12), and the inversion operation, E^*. The resulting symmetry labels (η and ϵ respectively) have been described in [10]. The symmetrized basis functions are

$$\psi_{ijkuw}^{\eta\epsilon} = [2(1 + \delta_{k0})]^{-1/2}\psi_i(R)[Y_{jk}(\theta, \phi) + (-1)^{k+\epsilon}Y_{j-k}(\theta, \phi)]\Phi_u(\cos\chi)\Upsilon_w(\rho), \quad (4)$$

where δ_{k0} is the Kronecker delta, and $u + k$ must be even for $(-1)^\eta = +1$ and odd for $(-1)^\eta = -1$.

The basis functions $\Upsilon_w(\rho)$ and $\Phi_u(\cos\chi)$ are defined to be eigenfunctions of 1-dimensional Hamiltonian operators for the coordinates concerned,

$$\hat{H}_\rho = -\frac{\hbar^2}{M_{\mathrm{Ar}}\rho}\left(\frac{\partial^2}{\partial\rho^2}\right)\rho + V_{\mathrm{eff}}(\rho) \quad (5)$$

and

$$\hat{H}_\chi = \left(\frac{\hbar^2}{M_{\mathrm{Ar}}\rho_{\mathrm{cut}}^2} + \frac{\hbar^2}{2\mu R_{\mathrm{cut}}^2}\right)\frac{\partial}{\partial\cos\chi}\left[(1 - \cos^2\chi)\frac{\partial}{\partial\cos\chi}\right] + V_{\mathrm{eff}}(\cos\chi). \quad (6)$$

In each case, the operator contains a one-dimensional effective potential V_{eff}. In [10], each V_{eff} was chosen to be a cut through the full potential energy surface for a fixed value of R, R_{cut}. The resulting basis functions in ρ are very well adapted to the lowest Ar–Ar bending and stretching states, but are less suitable for states with excitation in these modes. In the present work, we have used χ basis functions defined in the same way as before, but for ρ we have chosen to use functions that are slightly better at representing large-amplitude motions. For each value of ρ, a three-dimensional problem in R, θ and ϕ is solved, with χ fixed at 90°. This defines a set of adiabats $U_m(\rho)$. The Ar–Ar stretching basis functions $\Upsilon_w(\rho)$ are then taken to be eigenfunctions of the Hamiltonian of equation (5) with $V_{\mathrm{eff}}(\rho) = U_1(\rho)$.

The full Hamiltonian matrix is constructed in the non-orthogonal basis set of equation (4), as described in [10]. The resulting generalized eigenvalue problem is then solved using routines from the NAG Fortran Library [18]. This yields wavefunctions in the form

$$\Psi_n^{\eta\epsilon} = \sum_{ijkuw} c_{nijkuw}^{\eta\epsilon}\psi_{ijkuw}^{\eta\epsilon}, \quad (7)$$

which may then be used to calculate expectation values and spectroscopic intensities.

Rotational constants are calculated from the expectation values

$$B_x = \langle\hbar^2/(M_{\mathrm{Ar}}\rho^2\sin^2\chi) + \hbar^2/(2\mu R^2\tan^2\chi)\rangle; \quad (8)$$

$$B_y = \langle\hbar^2/2\mu R^2\rangle; \quad (9)$$

$$B_z = \langle\hbar^2/(2\mu R^2 + M_{\mathrm{Ar}}\rho^2)\rangle; \quad (10)$$

$$d_{xy} = \langle\hbar^2/(2\mu R^2\tan\chi)\rangle, \quad (11)$$

as described in [10]. This approach relies on an approximate separation of vibration

and rotation, and neglects the structure of the DCl molecule, treating it as a point mass. In addition, it omits any contributions to the rotational constants arising from Coriolis perturbations with other vibrational states. For this reason, the calculated rotational constants are considerably less reliable than the vibrational frequencies as a probe of the non-additive forces.

In addition to vibrational frequencies and rotational constants, the experiments provide nuclear quadrupole coupling constants χ_{xx}, χ_{yy} and χ_{zz}. The nuclear quadrupole coupling constants are related to angular expectation values by equations (1) and (2). These expectation values may be calculated straightforwardly from the wavefunctions as described in [10].

The dipole moment of the Ar_2–DCl complex is dominated by the permanent dipole of the DCl molecule. There are of course other contributions, from induced moments and overlap effects, but these are relatively small. To a good first approximation, the band intensities may be calculated in terms of matrix elements of a dipole moment operator of the form

$$\begin{aligned}
\mu_x^{\text{trimer}} &= \mu_{\text{DCl}} \cos\theta = \mu_{\text{DCl}} C_{10}(\theta, \phi); \\
\mu_y^{\text{trimer}} &= \mu_{\text{DCl}} \sin\theta \cos\phi = -2^{-1/2} \mu_{\text{DCl}} [C_{11}(\theta, \phi) - C_{1-1}(\theta, \phi)]; \\
\mu_z^{\text{trimer}} &= \mu_{\text{DCl}} \sin\theta \sin\phi = 2^{-1/2} i \mu_{\text{DCl}} [C_{11}(\theta, \phi) + C_{1-1}(\theta, \phi)],
\end{aligned} \tag{12}$$

where the C_{1q} are renormalized spherical harmonics in the body-fixed frame.

5. Intermolecular potentials

The complete intermolecular potential for Ar_2–HCl is made up of three parts: an Ar–HCl pair potential (which appears twice), an Ar–Ar pair potential, and a three-body term. This section will describe the pair potentials used for Ar–HCl and Ar–Ar, and the various contributions to the three-body potential.

5.1. *Pair potentials*

The Ar–Ar pair potential used in the present work is the HFD-C pair potential of Aziz and Chen [1], which was fitted to a wide range of experimental data and is known to give accurate vibrational frequencies and rotational constants for the Ar dimer. The Ar–HCl pair potential is the H6(4,3,0) potential [4], which was fitted to spectroscopic constants obtained from 25 different bands in the microwave, far-infrared and mid-infrared spectra of Ar–HCl and Ar–DCl. The H6(4,3,0) potential is a function of the HCl mass-reduced quantum number $\eta = (v + \frac{1}{2})/\mu_{\text{HCl}}^{1/2}$; the present work used the potential for DCl $v = 0$ throughout.

The Ar–HCl H6(4,3,0) potential is the most recent of a series of potentials fitted to vibration–rotation spectra of Ar–HCl and Ar–DCl. Recent measurements of the spectrum of Ar–DCl [19] have shown that predictions based on the H6(4,3,0) potential [4] are accurate to within $0{\cdot}25\,\text{cm}^{-1}$, even for states correlating with DCl $j = 2$; the $j = 2$ bands are sensitive to regions of the potential that were not sampled by the bands included in the original fit. The H6(4,3,0) predictions are at least a factor of 5 more accurate than those of its predecessor, the H6(3) potential [3], which gives predictions in error by up to $1{\cdot}7\,\text{cm}^{-1}$ for the Ar–DCl ($j = 2$) states. Despite this, it has been shown for Ar_2–HCl [10] that the HCl bending frequencies calculated on pairwise-additive H6(3) and H6(4,3,0) potentials differ by only $0{\cdot}4\,\text{cm}^{-1}$. It may

be concluded that, at a conservative estimate, the remaining uncertainties in the H6(4,3,0) potential may cause errors of up to $0{\cdot}3\,\mathrm{cm}^{-1}$ in the pairwise-additive bending frequencies for Ar_2–HCl and Ar_2–DCl.

The equilibrium geometry for Ar_2–DCl is near-equilateral, with $\chi = 90°$ and the D atom of DCl pointing between the two Ar atoms, $\theta = 0$. For the pairwise-additive potential, $R = 3{\cdot}49$ Å and $\rho = 3{\cdot}73$ Å at equilibrium. Contour plots of the pairwise-additive potential for Ar_2–HCl, which is very similar to that for Ar_2–DCl, have been given in figure 2 of [10].

5.2. *Non-additive contributions*

Various terms that contribute to the non-additive potential in a system such as Ar_2–HCl have been discussed in [10], and contour plots of their angle-dependence have been given in figure 6 therein. Only a brief summary will be given here.

5.2.1. *Dispersion contributions*

In atomic systems, the leading term in the 3-body dispersion interaction is the well-known Axilrod–Teller triple-dipole term, which takes the form [20]

$$V_{\mathrm{ddd}} = 3Z^{(3)}_{\mathrm{ddd}}\left(\frac{3\cos\theta_1\cos\theta_2\cos\theta_3 + 1}{r_1^3 r_2^3 r_3^3}\right), \tag{13}$$

where θ_1, θ_2 and θ_3 are the internal angles of the triangle formed by the three atoms and r_1, r_2 and r_3 are the corresponding distances. In molecular systems, the triple-dipole interaction is more complicated because of the anisotropy of molecular polarizabilities. The form of the triple-dipole energy under these circumstances has been given by Stogryn [21]. In the present work, the equations for the anisotropic triple-dipole interaction were evaluated using $\nu_{123} = 3Z^{(3)}_{ddd} = 1485E_h a_0^9$, extracted from the *ab initio* results of Chalasiński *et al.* [22], as described in [10], with $\alpha_{\mathrm{Ar}} = 11{\cdot}08\,a_0^3$ [23], $\alpha^{\parallel}_{\mathrm{HCl}} = 17{\cdot}234\,a_0^3$ and $\alpha^{\perp}_{\mathrm{HCl}} = 15{\cdot}414\,a_0^3$ [24]. The resulting energy was then damped using the damping function $D_{333}(r_1, r_2, r_3)$ given in equation (21) of [10]. The triple-dipole term gives a positive contribution to the interaction potential that is only weakly dependent on the DCl orientation at fixed R, but has rather more effect on the anisotropy of the well depth because of the variation in equilibrium distance with angle.

5.2.2. *Induced-dipole–induced-dipole contribution*

A further long-range three-body term arises from the interaction of the induced multipoles that develop on each of the two Ar atoms in the electrostatic field of the HCl molecule. In the present work, as in [10], the electrostatic field at each Ar atom was calculated using a single-centre multipole expansion for the HCl, including multipoles up to hexadecapole with values taken from the work of Bulanin *et al.* [25]. This gives a potential term that is considerably smaller than the triple-dipole term, but is explicity anisotropic, and favours in-plane over out-of-plane geometries.

5.2.3. *Short-range forces*

Short-range non-additive forces arising from two different sources were considered.

(i) Exchange overlap contribution. When two Ar atoms approach one another closely, their electron clouds distort away from one another in such a way as to reduce overlap. This distortion modifies their overlap with a third atom; if

the third atom is collinear with the first two, the overlap is increased and there is a positive contribution to the three-body energy. Conversely, for near-equilateral geometries, the deformation produces a negative contribution to the three-body energy. As in [10], this term was modelled using the first-order expression of Jansen (equation (37) of [26]), with range parameter $\beta_{eo} = 1{\cdot}24$ Å and an overall scaling factor $Z_{eo} = 0{\cdot}911$. Jansen's expression was actually derived for a triatomic system, so the HCl charge distribution is treated as spherically symmetric, centred at a point on the HCl axis, a distance δ_{eo} towards the H atom from the centre of mass. This gives an energy contribution that is only weakly anisotropic at fixed R, and is smaller than the triple-dipole term but of opposite sign. Again, it affects the well depth differently at different angles because of the angle-dependence of the equilibrium distance.

It may be noted that Jensen's original theory is known [27] to give a substantial overestimate of the short-range 3-body forces. However, although we have used Jansen's functional form, the parameters used were fitted to the *ab initio* calculations of Chalasiński *et al.* [22], so that the overall magnitude of the short-range forces is realistic. In particular, the range parameter β_{eo} used here is substantially larger than that suggested by Jansen for Ar_3.

(ii) Exchange multipole contribution. The exchange deformation of a pair of atoms, discussed in (i) above, generates a quadrupole moment on the Ar_2 pair. In a triatomic system, this produces a relatively small contribution to the non-additive forces, since the only effect on the energy is by interaction of the exchange quadrupole with the dipole moment it induces on the third atom (though the induced dipole itself is important, and is believed to be responsible for the absorption of far-infrared radiation by liquid rare gases [11]). In a complex such as Ar_2–HCl, however, the effect on the energy is much larger, because the exchange quadrupole generated on the Ar_2 pair can interact directly with the permanent multipole moments of the HCl molecule. Jansen [28] has described a simple model for the exchange quadrupole, which gives a function form

$$Q(\rho) = -\tfrac{1}{2}\rho^2 \frac{\exp(-\beta_{eq}^2\rho^2/2)}{1-\exp(-\beta_{eq}^2\rho^2/2)}. \tag{14}$$

As in [10], the parameter β_{eq} for Ar–Ar was taken to be $0{\cdot}965$ Å^{-1}, based on the *ab initio* calculations of Chalasiński *et al.* [22].

6. Computation results

The vibrational states that exist for Ar_2–DCl may be understood by comparison with those of Ar_3 and Ar–DCl. The correlation diagram is shown in figure 2. The DCl bending states were discussed qualitatively in the Introduction. However, before considering the convergence of the basis sets used in the present calculations, a more detailed understanding of the vibrations of the heavy-atom framework is needed.

In Ar_3, the lowest vibrationally excited states [29] are (i) a degenerate (E symmetry) pair involving χ bending motion and an asymmetric stretching motion, and (ii) a symmetric (breathing) stretch (A_1 symmetry). The bending vibrations are of large amplitude, but are reasonably well localized about a single equilateral geometry; the lowest E excited states lie about $22{\cdot}5$ cm^{-1} above the ground state, compared with

a barrier of about $100\,cm^{-1}$ to 'inversion' through a linear geometry. In an asymmetric molecule such as Ar_2–DCl or Ar_2–HCl, the degenerate pair is split into a χ bend (B_2 symmetry) and a 'wagging stretch' (A_1 symmetry), as described in [10]. In Ar_2–DCl, as in Ar_2–HCl, these two states appear about $25\,cm^{-1}$ above the ground state. The breathing stretch state (A_1 symmetry) is about $36\,cm^{-1}$ above the ground state, which is again similar to Ar_2–HCl.

The bending vibrational states of Ar_2–DCl execute lower-amplitude motion than those of Ar_2–HCl, because of the smaller rotational constant of DCl. For the pairwise-additive potential, the in-plane and out-of-plane bends lie about $30\,cm^{-1}$ and $36\,cm^{-1}$, respectively, above the ground state. Because of the larger anisotropy, the Σ bend is shifted further from its Ar–DCl value, and is predicted to be $44\,cm^{-1}$ above the ground state.

6.1. *Convergence tests*

For Ar_2–DCl, there are three different checks to be made concerning basis set convergence: (1) convergence of the basis set describing DCl internal rotation (θ and ϕ); (2) convergence of the basis set describing the pseudo-diatomic stretching

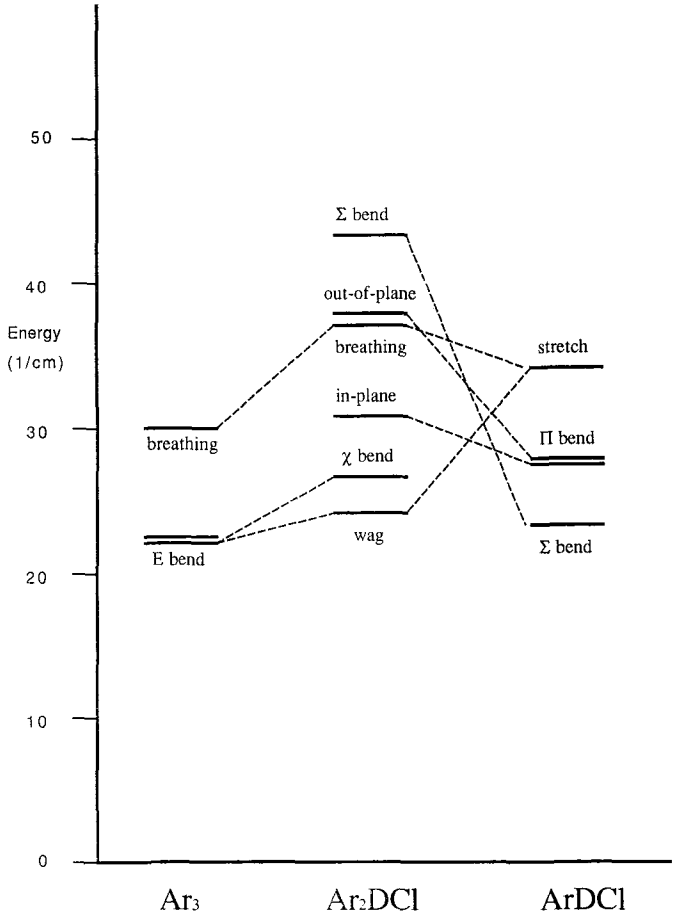

Figure 2. Correlation diagram comparing the vibrational energy levels of Ar_2–DCl with those of Ar_3 and Ar–DCl.

Table 3. Convergence of results for Ar_2–$D^{35}Cl$.

	$N_\rho = N_\chi = 1$; $N_i = 12$ ($R_{min} = 2{\cdot}75$ Å, $R_{max} = 4{\cdot}35$ Å)					
	Ground state			Out-of-plane bend		
j_{max}	E/cm^{-1}	$\langle P_2(\cos\theta)\rangle$	B_y/MHz	E/cm^{-1}	$\langle P_2(\cos\theta)\rangle$	B_y/MHz
3	−325·875	0·5527	1649·6	−287·764	0·1018	1679·7
4	−326·575	0·5853	1648·1	−289·384	0·1798	1676·8
5	−326·696	0·5920	1647·8	−289·742	0·2009	1675·7
6	−326·713	0·5926	1647·8	−289·802	0·2045	1675·5
7	−326·716	0·5927	1647·8	−289·810	0·2048	1675·7
5*	−326·672	0·5919	1647·9	−289·708	0·2007	1675·9
6*	−326·684	0·5926	1647·9	−289·755	0·2042	1675·7
	$N_\rho = N_\chi = 1$; $j_{max} = 6$* angular basis; $R_{min} = 2{\cdot}75$ Å, $R_{max} = 4{\cdot}35$ Å					
	Ground state			Breathing stretch		
N_i	E/cm^{-1}	$\langle P_2(\cos\theta)\rangle$	B_y/MHz	E/cm^{-1}	$\langle P_2(\cos\theta)\rangle$	B_y/MHz
10	−326·679	0·5930	1647·3	−290·549	0·5708	1589·9
12	−326·684	0·5926	1647·9	−290·709	0·5712	1592·9
14	−326·684	0·5927	1648·1	−290·710	0·5711	1593·0
16	−326·684	0·5928	1647·9	−290·710	0·5716	1593·1
16[a]	−326·684	0·5926	1648·0	−290·710	0·5713	1593·0

* Reduced basis set ($k = 4$ not included for $j = 4$, $k > 1$ not included for $j > 4$).
[a] $R_{min} = 2{\cdot}5$ Å, $R_{max} = 4{\cdot}6$ Å.

coordinate (R); and (3) convergence of the basis set describing the heavy-atom motions (ρ and χ). Since the Ar_2–DCl intermolecular vibration observed experimentally in this work correlates with hindered internal rotation of DCl (as do the other transitions likely to be observed experimentally in the future), it is particularly important to use as complete a basis set as possible in these coordinates. The convergence of calculations on the ground state and the out-of-plane bend with respect to j_{max} and k_{max} is illustrated in table 3, for $N_i = 12$ and a single basis function for each of the ρ and χ motions. These states were chosen both because they are the ones of immediate experimental interest and because the out-of-plane bend correlates with $k \neq 0$, and therefore provides a more stringent test of the convergence. It may be seen that the vibrational frequencies are converged to $\pm 0{\cdot}02$ cm^{-1} and the expectation values to $\pm 0{\cdot}0005$ for $j_{max} = 6$. In the previous Ar_2–HCl work, a reduced basis set with $j_{max} = 5$, but excluding the $j = 4$, $k = 4$ and $j = 5$, $k > 1$ functions, was chosen since its convergence properties were almost as good as for the full $j_{max} = 5$ basis set. We have followed the same approach for Ar_2–DCl, and found that a reduced basis set, with $j_{max} = 6$ but excluding functions with $j = 4$, $k = 4$ and $j > 4$, $k > 1$, provides a reasonable compromise between convergence properties and basis set size. This basis set is denoted 6*, and is used throughout the remainder of this paper. Results using the same basis set as for Ar_2–HCl (denoted 5*) are also included in table 3. As expected, the convergence with respect to j_{max} is somewhat slower for Ar_2–DCl than for Ar_2–HCl, because of the smaller rotational constant of DCl.

The convergence with respect to the number of distributed Gaussians N_i is also

illustrated in table 3, for the $j_{max} = 6^*$ basis set, again with only one basis function in ρ and χ. It is found that a basis of 12 functions provides excellent convergence, and that an integration interval with $R_{min} = 2{\cdot}75$ Å and $R_{max} = 4{\cdot}35$ Å is adequate. This may be compared with the larger basis and integration interval used for the Ar_2–HCl calculations ($N_i = 16$ and $R_{min} = 2{\cdot}5$ Å and $R_{max} = 4{\cdot}6$ Å respectively), which was probably larger than necessary. The basis set with $N_i = 12$ was used throughout the remainder of this paper.

As noted for Ar_2–HCl, restrictions on computer power make testing convergence for the ρ and χ coordinates very difficult. However, the new scheme described for constructing the ρ basis does result in considerably faster convergence. Using a basis consisting of 4 functions in ρ and 5 in χ, with $q_{max} = 4$, we estimate that the fundamental bending and stretching vibrations associated with the heavy-atom coordinates are converged to within $\pm 0{\cdot}02\,cm^{-1}$, while the overtones and combination states are converged to within a few cm^{-1}. This basis set will be used throughout the remainder of this paper. The experimental results for Ar_2–HCl [9] indicate the possibility of Coriolis coupling between a stretch overtone and the out-of-plane bend, so that it is desirable to attempt to calculate these levels as accurately as possible. This will be an even more important consideration for Ar_2–HF, since even the lowest excited HF bending states will lie in this heavy-atom overtone region.

6.2. *Calculations on pairwise-additive and non-additive potentials*

The results of calculations on the pairwise-additive and non-additive potentials are shown in table 4, and compared with the experimental results for the ground and out-of-plane bending states. The calculations used the full basis set described in section 6.1 above. It may be seen that the pairwise-additive potential overestimates the out-of-plane bending frequency by $1{\cdot}4\,cm^{-1}$. This discrepancy is about a factor of 5 larger than can be attributed to uncertainties in the Ar–Ar and Ar–HCl pair potentials. The three-body potential used here actually overcorrects this discrepancy somewhat, and underestimates the frequency by $0{\cdot}8\,cm^{-1}$. This overestimate of the correction is in agreement with the results for Ar_2–HCl in [10].

The three-body potential also overcorrects the discrepancies in $\langle P_2(\cos\theta)\rangle$ for both states, and brings the ground-state value of $\langle\Delta(\theta,\phi)\rangle$ into good agreement with experiment. The ground-state rotational constants are also improved. There are clearly some problems with the excited-state rotational constants, but these may be attributed mostly to the neglect of Coriolis coupling in the calculations rather than to inadequacy of the three-body potential.

We have also calculated the overall band intensities for the various far-infrared bands originating in the ground state, and the results are included in table 4. As described above, these calculations are based on the approximation that the dipole moment function of the complex is due solely to the dipole of the DCl monomer, as in equation (12). The results suggest that the in-plane bend should have similar intensity to the out-of-plane bend, and should thus be observable. However, the Σ bend is a factor of 15 less intense, and will be much more difficult to observe. This arises because of the poor Franck–Condon overlap between the ground and Σ bend excited states in Ar_2–DCl, which are concentrated at $\theta = 0$ and 180°, respectively. The Σ bend intensity is much lower for Ar_2–DCl than for Ar_2–HCl, because of the smaller rotational constant and bending amplitude for DCl. In a near-rigid picture of the bending motion, the Σ bend correlates with the first overtone of the bend, and is

Table 4. Results of calculations from pairwise-additive and three-body potentials and observed values.

Ar_2–$D^{35}Cl$	Pairwise-additive	Pairwise-additive + three-body	Observed
Ground state (A_1 symmetry)			
Binding energy/cm^{-1}	−328·400	−316·681	
B_x/MHz	1759·97	1730·05	1735·0953
B_y/MHz	1659·66	1656·45	1651·6647
B_y/MHz	847·26	839·01	840·5010
$\langle P_1(\cos\theta)\rangle$	0·8378	0·8209	
$\langle P_2(\cos\theta)\rangle$	0·5933	0·5589	0·566583
$\langle \Delta(\theta,\phi)\rangle$	0·0225	0·0325	0·032420
In-plane bend (B_2 symmetry)			
ν_0/cm^{-1}	31·243	28·193	
B_x/MHz	1753·83	1741·35	
B_y/MHz	1638·02	1616·13	
B_z/MHz	838·44	828·12	
$\langle P_1(\cos\theta)\rangle$	0·6474	0·6527	
$\langle P_2(\cos\theta)\rangle$	0·2445	0·2737	
$\langle \Delta(\theta,\phi)\rangle$	0·2467	0·2132	
Band intensity	0·11167	0·09013	
Out-of-plane bend (B_1 symmetry)			
ν_0/cm^{-1}	37·437	35·223	36·04605
B_x/MHz	1753·48	1732·08	1788·14
B_y/MHz	1685·37	1680·75	1662·76
B_z/MHz	852·13	845·49	849·021
$\langle P_1(\cos\theta)\rangle$	0·6316	0·5935	
$\langle P_2(\cos\theta)\rangle$	0·2062	0·1579	0·189
$\langle \Delta(\theta,\phi)\rangle$	−0·2426	−0·2488	−0·226
Band intensity	0·11929	0·12461	
Σ bend (A_1 symmetry)			
ν_0/cm^{-1}	44·225	39·500	
B_x/MHz	1749·07	1739·00	
B_y/MHz	1742·86	1724·09	
B_z/MHz	864·61	857·07	
$\langle P_1(\cos\theta)\rangle$	−0·4996	−0·3977	
$\langle P_2(\cos\theta)\rangle$	0·2522	0·1896	
$\langle \Delta(\theta,\phi)\rangle$	0·1192	0·1506	
Band intensity	0·00785	0·01262	
Wagging stretch (A_1 symmetry)			
ν_0/cm^{-1}	24·986	23·346	
B_x/MHz	1662·44	1630·37	
B_y/MHz	1700·06	1701·25	
B_y/MHz	825·77	816·93	
$\langle P_1(\cos\theta)\rangle$	0·8313	0·8179	
$\langle P_2(\cos\theta)\rangle$	0·5822	0·5535	
$\langle \Delta(\theta,\phi)\rangle$	0·0244	0·0335	
Band intensity	0·00008	0·00003	
χ bend (B_2 symmetry)			
ν_0/cm^{-1}	26·022	24·225	
B_x/MHz	1784·49	1753·44	
B_y/MHz	1625·03	1639·80	
B_z/MHz	837·80	835·48	
$\langle P_1(\cos\theta)\rangle$	0·8066	0·7443	
$\langle P_2(\cos\theta)\rangle$	0·5311	0·4193	

Table 4. Continued

$Ar_2D^{35}Cl$	Pairwise-additive	Pairwise-additive + three-body	Observed
χ bend (continued)			
$\langle\Delta(\theta,\phi)\rangle$	0·0658	0·1334	
Band intensity	0·02996	0·06720	
Breathing stretch (A_1 symmetry)			
ν_0/cm^{-1}	36·651	35·347	
B_x/MHz	1734·97	1705·82	
B_y/MHz	1607·51	1610·26	
B_z/MHz	823·42	816·19	
$\langle P_1(\cos\theta)\rangle$	0·8273	0·7855	
$\langle P_2(\cos\theta)\rangle$	0·5721	0·5234	
$\langle\Delta(\theta,\phi)\rangle$	0·0243	0·0386	
Band intensity	0·00005	0·00066	

therefore forbidden; Ar_2–DCl is closer to this limit than Ar_2–HCl, so that the Σ bend is weaker for Ar–DCl.

As expected, the heavy-atom vibrational transitions are mostly weak compared with the strongly allowed in- and out-of-plane transitions. This indicates that the potential introduces little mixing of these states with the DCl bending levels. However, one exception to this is the χ bend, which is of the same symmetry as the in-plane DCl bend; the χ bend borrows some intensity and is predicted to have about 25% of the intensity of the in-plane bend for the pairwise-additive potential. For the non-additive potential, the intensity of the χ bend is increased by more than a factor of two, because of increased mixing with the closer-lying in-plane bend. It should be possible to observe this state experimentally, and obtain the first direct information on the heavy-atom vibrations in the Ar_2–H(D)Cl systems.

6.3. *Contributions from individual non-additive terms*

It is of particular interest to investigate which of the various three-body forces included in the model affect the experimental spectra most strongly. To facilitate this, the separate contributions to the various spectroscopic observables from each three-body term are compiled in table 5.

The well-known Axilrod–Teller triple-dipole term has long been included as the sole 'three-body correction' in the fitting of various bulk experimental data in rare gas systems. In molecular systems, the triple-dipole term is anisotropic, as mentioned above. Nevertheless, table 5 shows that, for the bending frequencies of interest here, the triple-dipole term makes a relatively small contribution to the total three-body correction (though the effect on the binding energy is much larger). The triple-dipole term is not adequate for a reconciliation of the discrepancy with experimental results.

The induced-dipole–induced-dipole three-body term is intrinsically anisotropic, and thus influences the spectroscopic observables more directly. Although the induced-dipole–induced-dipole term contributes a much smaller correction to the binding energy than the triple-dipole term, its effect on the spectroscopic observables is comparable. However, the total effect of the induced-dipole–induced-dipole term is still too small to reconcile the observed differences between experiment and theory.

The exchange overlap contributions, which for some atomic systems have been

Table 5. Changes in calculated spectroscopic parameters for Ar_2–$D^{35}Cl$ when different 3-body terms are added to the pairwise-additive potential.

Ar_2–$D^{35}Cl$	Triple-dipole	Induced-dipole induced dipole	Exchange overlap	Exchange quadrupole	Sum of changes	All terms together
Ground state (A_1)						
Binding energy/cm^{-1}	7·230	0·973	−0·711	4·476	11·968	11·719
B_x/MHz	−9·84	−1·78	2·06	−20·51	−30·07	−29·92
B_y/MHz	−6·47	−0·56	1·67	1·66	−3·70	−3·21
B_z/MHz	−4·14	−0·59	0·92	−4·59	−8·40	−8·25
$\langle P_1(\cos\theta)\rangle \times 10^3$	−0·3	−3·4	0·0	−12·4	−16·1	−16·9
$\langle P_2(\cos\theta)\rangle \times 10^3$	−2·2	−7·7	0·2	−24·6	−39·8	−34·4
$\langle \Delta(\theta,\phi)\rangle \times 10^3$	1·4	2·1	−0·2	6·4	9·7	10·0
In-plane bend (B_2)						
ν_0/cm^{-1}	−0·582	−0·684	0·097	−2·243	−3·412	−3·050
B_x/MHz	−11·56	0·94	2·38	−4·51	−12·75	−12·48
B_y/MHz	−2·38	−4·15	0·94	−13·24	−18·83	−21·89
B_z/MHz	−3·27	−1·16	0·80	−5·73	−9·36	−10·32
$\langle P_1(\cos\theta)\rangle \times 10^3$	−7·7	3·5	1·0	16·3	13·1	5·3
$\langle P_2(\cos\theta)\rangle \times 10^3$	−14·7	8·4	1·9	18·7	14·3	29·2
$\langle \Delta(\theta,\phi)\rangle \times 10^3$	11·0	−7·7	−1·2	−26·4	−24·3	−33·5
Out-of-plane bend (B_1)						
ν_0/cm^{-1}	0·002	−0·464	−0·004	−1·863	−2·329	−2·214
B_x/MHz	−10·25	−0·99	2·27	−12·17	−21·14	−21·40
B_y/MHz	−7·37	−0·24	1·82	1·23	−4·56	−4·62
B_z/MHz	−4·50	−0·31	1·01	−2·73	−6·53	−6·64
$\langle P_1(\cos\theta)\rangle \times 10^3$	−3·2	−4·6	0·5	−31·9	−39·2	−38·1
$\langle P_2(\cos\theta)\rangle \times 10^3$	−3·7	−7·2	0·8	−40·1	−50·2	−48·3
$\langle \Delta(\theta,\phi)\rangle \times 10^3$	0·4	−0·9	0·0	−6·4	−6·9	−6·2
Σ bend (A_1)						
ν_0/cm^{-1}	0·410	−0·874	0·109	−4·703	−5·058	−4·725
B_x/MHz	−12·51	−0·09	2·96	0·24	−9·40	−10·07
B_y/MHz	−14·61	0·32	0·96	−7·11	−20·44	−18·77
B_z/MHz	−6·92	0·04	0·98	−1·94	−7·84	−7·54
$\langle P_1(\cos\theta)\rangle \times 10^3$	63·8	−5·6	−0·4	54·7	112·5	100·9
$\langle P_2(\cos\theta)\rangle \times 10^3$	−44·2	5·6	0·5	−24·9	−63·0	−62·6
$\langle \Delta(\theta,\phi)\rangle \times 10^3$	13·5	−0·6	0·1	18·8	31·8	31·4
Wagging stretch (A_1)						
ν_0/cm^{-1}	−0·720	−0·129	0·073	−0·903	−1·679	−1·640
B_x/MHz	−11·90	−1·96	1·75	−19·66	−31·77	−32·07
B_y/MHz	−4·57	−0·27	1·65	3·54	0·35	1·19
B_z/MHz	−4·50	−0·63	0·87	−4·72	−8·98	−8·84
$\langle P_1(\cos\theta)\rangle \times 10^3$	−1·1	−3·1	0·0	−9·6	−13·8	−13·4
$\langle P_2(\cos\theta)\rangle \times 10^3$	−2·8	−7·0	0·2	−20·0	−29·6	−28·7
$\langle \Delta(\theta,\phi)\rangle \times 10^3$	1·7	2·1	−0·1	5·5	9·2	9·1
χ bend (B_2)						
ν_0/cm^{-1}	−0·420	−0·217	−0·030	−0·926	−1·593	−1·797
B_x/MHz	−7·57	−3·04	1·93	−22·70	−31·38	−31·05
B_y/MHz	−11·47	3·88	2·37	16·60	11·38	14·77
B_z/MHz	−5·20	0·57	1·11	0·10	−3·42	−2·32
$\langle P_1(\cos\theta)\rangle \times 10^3$	4·8	−11·0	−0·8	−50·4	−57·4	−62·3
$\langle P_2(\cos\theta)\rangle \times 10^3$	9·4	−21·1	−1·2	−88·2	−101·1	−111·8
$\langle \Delta(\theta,\phi)\rangle \times 10^3$	−7·2	12·8	0·9	52·9	59·4	67·6

Table 5. Continued

Ar_2–$D^{35}Cl$	Triple dipole	Induced-dipole induced dipole	Exchange overlap	Exchange quadrupole	Sum of changes	All terms together
Breathing stretch (A_1)						
ν_0/cm^{-1}	−0·625	−0·129	0·021	−0·610	−1·343	−1·304
B_x/MHz	−10·13	−1·82	2·25	−19·23	−28·93	−29·15
B_y/MHz	−6·71	0·03	1·68	7·69	2·69	2·75
B_z/MHz	−4·70	−0·51	1·02	−2·97	−7·16	−7·23
$\langle P_1(\cos\theta)\rangle \times 10^3$	−1·0	−5·1	−0·4	−44·1	−50·6	−41·8
$\langle P_2(\cos\theta)\rangle \times 10^3$	−1·9	−8·4	0·0	−41·3	−51·6	−48·7
$\langle \Delta(\theta,\phi)\rangle \times 10^3$	2·1	2·4	−0·1	10·6	15·0	14·3

suggested to be of equal magnitude but opposite sign to the triple-dipole term, have little effect on the spectroscopic properties of Ar_2–DCl. It is clear that the traditional approach of considering the degree of cancellation between the triple-dipole and exchange-overlap terms as an estimate of the uncertainty in the three-body forces is not appropriate in molecular systems such as Ar_2–HCl.

The exchange multipole contributions are seen to be quite large and anisotropic, and are responsible for most of the three-body shifts in the calculated spectroscopic properties. Indeed, this term seems to overcorrect the pairwise-additive results with respect to the experimentally measured properties. However, the model used for the exchange quadrupole term in the present work is far from quantitative, and was simply intended to give a rough idea of its magnitude and functional form. It is clear that a more accurate modelling of this term will be necessary for future calculations.

To summarize the effect of the 3-body terms, it may be seen that, for the ground state, the sum of the terms discussed above produces good agreement with experiment for both the rotational constants and angular expectation values. For the out-of-plane bend, the experimental band origin and $\langle P_2(\cos\theta)\rangle$ are bracketed by the calculations on the pairwise-additive and complete non-additive potentials, indicating that the 3-body terms are probably too large for values of θ further from equilibrium. The experimental rotational constants for the out-of-plane bend are likely to contain relatively large contributions from Coriolis coupling (as was discussed earlier in the analysis of the experimental data) and therefore cannot be compared meaningfully with the calculated rotational constants. All these conclusions—good agreement for ground-state constants, over-correction of bending frequencies, and non-structural excited-state rotational constants—are similar to those obtained previously for Ar_2–HCl [10].

7. Conclusions

We have observed the out-of-plane DCl bending band of the Ar_2–DCl van der Waals trimer, using tunable far-infrared laser spectroscopy in a planar supersonic expansion. We have assigned the rotational and ^{35}Cl nuclear hyperfine structure, and obtained full information on the vibrational and rotational energy levels.

We have performed dynamical calculations on Ar_2–DCl, explicitly taking account of all five low-frequency vibrational degrees of freedom. Calculations were performed using both pairwise-additive potentials and a variety of non-additive corrections.

There are significant discrepancies between the experimental results and calculations based on the pairwise-additive potential, demonstrating that the effects of non-additivity are important. In particular, the pairwise-additive potential overestimates the out-of-plane bending frequency by $1{\cdot}4\,cm^{-1}$, which is about a factor of 5 larger than can be attributed to uncertainties in the pair potentials.

Several different non-additive interactions have been investigated. Non-additive dispersion interactions, induced-dipole–induced-dipole interactions and exchange overlap interactions were all found to be significant, but not large enough to resolve the discrepancy between theory and experiment. However, as for Ar_2–HCl [10], the interaction between the permanent HCl multipoles and the exchange quadrupole developed by a pair of Ar atoms at short range was found to be more important. Including this interaction gave good agreement between experiment and theory for the ground-state properties, and over-corrected slightly for the discrepancy between the experimental and theoretical out-of-plane bending frequencies.

We have also given predictions of the spectra of other excited vibrational states, some of which should be experimentally observable. It would be particularly interesting to observe the χ bending state, because this would provide the first information on heavy-atom vibrational modes in atom–atom–diatom complexes. By combining results from the spectroscopy of Ar_2–HCl and Ar_2–DCl, it should be possible to use the experimental spectroscopic data to adjust the parameters of the non-additive contributions, and thus obtain direct information on non-additive forces in molecular systems.

This work was supported by the National Science Foundation (Grant #CH-9123335) and by the Science and Engineering Research Council. The authors are grateful to the NATO Collaborative Research Grant programme for travel funds. M.J.E. thanks the University of California for a graduate fellowship.

References

[1] Aziz, R. A., and Chen, H. H., 1977, *J. chem. Phys.*, **67,** 5719.
[2] Aziz, R. A., and Slaman, M. J., 1986, *Molec. Phys.*, **58,** 679.
[3] Hutson, J. M., 1988, *J. chem. Phys.*, **89,** 4550.
[4] Hutson, J. M., 1992, *J. phys. Chem.*, **96,** 4237.
[5] Klots, T. D., Chuang, C., Ruoff, R. S., Emilsson, T., and Gutowsky, H. S., 1987, *J. chem. Phys.*, **86,** 5315.
[6] Hutson, J. M., Beswick, J. A., and Halberstadt, N., 1989, *J. chem. Phys.*, **90,** 1337.
[7] Elrod, M. J., Steyert, D. W., and Saykally, R. J., 1991, *J. chem. Phys.*, **94,** 58.
[8] Elrod, M. J., Steyert, D. W., and Saykally, R. J., 1991, *J. chem. Phys.*, **95,** 3182.
[9] Elrod, M. J., Loeser, J. G., and Saykally, R. J., 1993, *J. chem. Phys.*, **98,** 5352.
[10] Cooper, A. R., and Hutson, J. M., 1993. *J. chem. Phys.*, **98,** 5337.
[11] Guillot, B., Mountain, R. D., and Birnbaum, G., 1988, *Molec. Phys.*, **64,** 747.
[12] Klots, T. D., and Gotowsky, H. S., 1989, *J. chem. Phys.*, **91,** 63.
[13] Blake, G. A., Laughlin, K. B., Busarow, K. L., Cohen, R. C., Gwo, D.-H., Schmuttenmaer, C. A., Steyert, D. W., and Saykally, R. J., 1991, *Rev. Sci. Instrum.*, **62,** 1693, 1701.
[14] Shoemaker, D. P., Garland, C. W., Nibler, J. W., 1989, *Experiments in Physical Chemistry,* 5th Edn (McGraw-Hill).
[15] Watson, J. K. G., 1967, *J. chem. Phys.*, **21,** 156.
[16] Benz, H. P., Bauder, A., and Gunthard, H. H., 1966, *J. molec. Spectrosc.*, **21,** 156.
[17] Hamilton, I. P., and Light, J. C., 1986, *J. chem. Phys.*, **84,** 306.
[18] NAG Fortran Library, Mark 14, 1990 (Numerical Algorithms Group Ltd., Oxford, UK)

[19] Elrod, M. J., Host, B. C., Steyert, D. W., and Saykally, R. J., 1993, *Molec. Phys.*, **79,** 245.
[20] Axilrod, B. M., and Teller, E., 1943, *J. chem. Phys.*, **11,** 299.
[21] Stogryn, D. E., 1970, *Phys. Rev. Lett.*, **24,** 971.
[22] Chałasiński, G., Szczesniak, M. M., and Kukawska-Tarnawska, B., 1991, *J. chem. Phys.*, **94,** 6677.
[23] Kumar, A., and Meath, W. J., 1984. *Can. J. Chem.*, **63,** 1616.
[24] Lazzeretti, P., Rossi, E., and Zanasi, R., 1981, *J. Phys. B*, **14,** L269.
[25] Bulanin, M. O., Bulychev, V. P., and Tokhadze, K. G., 1987. *J. molec. Spectrosc.*, **161,** 321.
[26] Jansen, L., 1965, *Adv. Quantum Chem.*, **2,** 119.
[27] Meath, W. J., and Aziz, R. A., 1984, *Molec. Phys.*, **52,** 225.
[28] Jansen, L., 1962, *Phys. Rev.*, **125,** 1798.
[29] Cooper, A. R., Jain, S., and Hutson, J. M., 1993, *J. chem. Phys.*, **98,** 2160.